CORONAVIRUS

Unexpected air pollution with marked emission reductions during the COVID-19 outbreak in China

Tianhao Le[1]*, Yuan Wang[1]*†, Lang Liu[2,3]*, Jiani Yang[1], Yuk L. Yung[1], Guohui Li[2,3], John H. Seinfeld[4]

The absence of motor vehicle traffic and suspended manufacturing during the coronavirus disease 2019 (COVID-19) pandemic in China enabled assessment of the efficiency of air pollution mitigation. Up to 90% reduction of certain emissions during the city-lockdown period can be identified from satellite and ground-based observations. Unexpectedly, extreme particulate matter levels simultaneously occurred in northern China. Our synergistic observation analyses and model simulations show that anomalously high humidity promoted aerosol heterogeneous chemistry, along with stagnant airflow and uninterrupted emissions from power plants and petrochemical facilities, contributing to severe haze formation. Also, because of nonlinear production chemistry and titration of ozone in winter, reduced nitrogen oxides resulted in ozone enhancement in urban areas, further increasing the atmospheric oxidizing capacity and facilitating secondary aerosol formation.

The abrupt outbreak of the coronavirus disease 2019 (COVID-19) pandemic produced previously unseen societal impacts in China. To curb the virus spread among humans, a preventive lockdown was first implemented on 23 January in Wuhan, Hubei. Other major cities and counties in China subsequently followed suit, and the entire nation's lockdown lasted for at least 3 weeks (varying in different regions). During the lockdown period, emissions from the traffic sector were markedly reduced. Such a shutdown serves as a natural experiment to evaluate air-quality responses to a marked emissions reduction and to assess the interplay between emission, atmospheric chemistry, and meteorological conditions. In this work, we synthesize multiple-year satellite-retrieved atmospheric compositions, national ground-station measurements of major pollutants, meteorology from reanalysis data, and a suite of state-of-the-art online atmospheric chemistry model simulations to assess the atmospheric influence of the COVID-19 outbreak in China and to reveal its implications for air pollution control strategies.

China has continued to battle particulate haze pollution (*1*). Long-term regulatory plans targeting energy and industrial emissions have been implemented (*2*), and nationwide improvement of fine particulate matter (PM) levels has been reported (*3*). Nonetheless, the key chemical and physical processes responsible for severe haze formation in China remain elusive, including exacerbated ozone levels (*4*, *5*), pathways of secondary aerosol formation (*6*, *7*), and emissions-meteorology interactions (*8*). Certain societal events in China with short-term stringent emission controls have been studied as natural experiments, such as the "Olympic Blue" during the 2008 Beijing Summer Olympic Games (*9*) and the "APEC Blue" during the 2014 Asia-Pacific Economic Cooperation (APEC) Economic Leaders' Meetings in Beijing (*10*, *11*). Emission controls during these two events resulted in a 40 to 60% reduction in SO_2, NO_2, nonmethane volatile organic compounds (VOCs), and PM.

The primary focus period during the COVID-19 lockdown in China was from 23 January to 13 February 2020 (hereafter referred to as the 2020-CLD period). This period encompassed a 7-day national holiday traditionally celebrating the Lunar New Year, during which previous studies have noted the reduction in anthropogenic emissions (*12*). NO_2 is key in atmospheric chemistry and serves as an important precursor for both ozone production and secondary aerosol formation (*6*, *13*). Changes in NO_2 during the lockdown period can be assessed by comparing spaceborne NO_2 measurements in the same time periods over different years. The TROPOspheric Monitoring Instrument (TROPOMI) on board the Copernicus Sentinel-5 Precursor satellite has provided key trace gas measurements of high accuracy since 2018. TROPOMI data show a quite low amount of column-integrated NO_2 during the 2020-CLD, with a mean value of 1.72 mg m^{-2}, and general uniformity throughout the whole country (Fig. 1A). By contrast, in the same period in 2019, hotspots of NO_2 were evident over eastern China, where the regional mean NO_2 abundance was four to five times higher than that in other regions of China (Fig. 1B). Regional means over eastern China experienced a reduction of 5.70 mg m^{-2} in NO_2, corresponding to a −71.9% fractional change (Fig. 1C). At the peak of the disease outbreak, Wuhan experienced a 93% fractional reduction in NO_2. Such a short-term human-induced reduction in NO_2 has been previously unseen, well exceeding the previous 2014 APEC Blue,

[1]Division of Geological and Planetary Sciences, California Institute of Technology, Pasadena, CA, USA. [2]State Key Laboratory of Loess and Quaternary Geology, Institute of Earth Environment, Chinese Academy of Sciences, Xi'an, Shaanxi, China. [3]Key Lab of Aerosol Chemistry and Physics, Institute of Earth Environment, Chinese Academy of Sciences, Xi'an, Shaanxi, China. [4]Divisions of Chemistry and Chemical Engineering and Engineering and Applied Science, California Institute of Technology, Pasadena, CA, USA.
*These authors contributed equally to this work.
†Corresponding author. Email: yuan.wang@caltech.edu

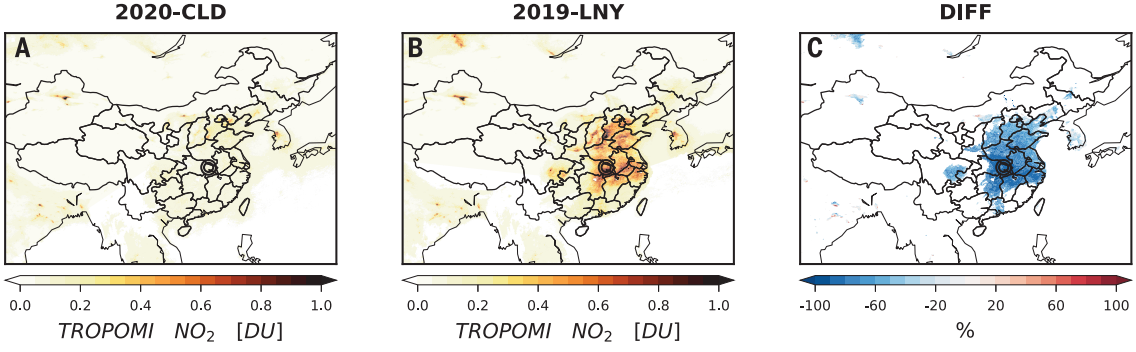

Fig. 1. Spaceborne measurements of NO_2 from TROPOMI. (**A**) Column-integrated NO_2 averaged over the 2020-CLD period for 3 weeks during 23 January to 13 February 2020. (**B**) Column-integrated NO_2 averaged over the reference period in 2019. To account for the annual holiday, the 2019 reference period we choose is the same as that in 2020-CLD in the Chinese lunar calendar, including the Chinese Lunar New Year (2019-LNY). TROPOMI NO_2 is available only starting from June 2018. (**C**) The fractional changes (DIFF) between (A) and (B), calculated only for the regions with NO_2 in 2019-LNY greater than 0.2 Dobson units (DU). The symbols in the maps indicate the location of Wuhan, the city most affected by COVID-19. 1 DU = 0.4462 mmol m^{-2}.

with the largest NO_2 reduction of ~40% (*10*). Compared with a 5-year climatology (2015 to 2019) based on the NASA Aura Ozone Monitoring Instrument, the NO_2 reductions mainly occurred over the North China plain (fig. S1).

In addition to spaceborne retrievals, we explore surface measurements of fine-mode aerosols and trace gas species over the entire region of eastern China (fig. S2). We calculate separately the climatological means of the past 5 years (2015 to 2019) during the same 3-week period as the 2020-CLD, including the Lunar New Year (hereafter referred to as CLIM-LNY) and the same 3-week period in the Georgian calendar (CLIM). The difference between CLIM-LNY and CLIM is attributed mainly to the holiday effect. In Wuhan, surface concentrations of NO_2 and SO_2 were the lowest compared with the 3-week means before the 2020-CLD as well as the climatological means over the past 5 years. $PM_{2.5}$ (PM with aerodynamic diameter less than 2.5 μm) was reduced by 23.2 μg m^{-3} (–32.4%) and 37.4 μg m^{-3} (–43.5%) as compared with CLIM-LNY and CLIM, respectively (Fig. 2A). In contrast to the changes to the $PM_{2.5}$, the surface ozone mixing ratio showed an enhancement of +5.0 parts per billion (ppb) (+25.1%) in Wuhan during the 2020-CLD as compared with CLIM-LNY. Ozone chemistry is highly nonlinear, and in the winter in urban areas in China, its production is in a NO_x-saturated regime (NO_x = NO + NO_2) because of the relative lack of HO_x radicals (*13*). Besides, reduction of fresh NO emissions alleviates ozone titration (*13*, *14*). Thus, a reduction of NO_x leads to an increase in ozone. Previous studies also attributed the anticorrelation between $PM_{2.5}$ and ozone to the aerosol radiative effect on the photochemistry of ozone formation (*4*, *15*), as well as the aerosol sink for ozone precursors (*5*). Changes in gaseous and particulate levels in the major cities of southern China, Guangzhou (Fig. 2C) and Shanghai (Fig. 2D), resemble those of Wuhan during the city lockdown.

In contrast to southern and central China, $PM_{2.5}$ in northern China during the outbreak period increased substantially (Fig. 2B). During the 3 weeks of 2020-CLD, several severe haze events occurred in Beijing with the maximum daily $PM_{2.5}$ level of 273.8 μg m^{-3}. The 2020-CLD mean surface $PM_{2.5}$ in Beijing increased by 16.3 μg m^{-3} (+23.4%) and 30.6 μg m^{-3} (+55.1%) in comparison with CLIM-LNY and CLIM, respectively (Fig. 2B). Nonetheless, NO_2 and SO_2 remained the lowest among the past 6 years, similar to that of the southern cities. Response of ozone concentration in Beijing followed a similar trend as that of $PM_{2.5}$, reaching a peak during the 2020-CLD. Daytime relationships between NO_2 and ozone concentrations in the winter of northern China show remarkable ozone titration during daytime, particularly with increasing $PM_{2.5}$, which further attenuates the incoming solar radiation, but the titration effect becomes considerably alleviated during the city lockdown (fig. S3). Nationwide, 1515 state monitoring stations show clear hotspots of surface $PM_{2.5}$ over northern China during the 2020-CLD (Fig. 2E), although the national mean of the 2020-CLD $PM_{2.5}$ was 52.1 μg m^{-3}, which falls in the 1σ range of variation of national climatology, 54.7 ± 6.1 μg m^{-3}. Satellite-observed aerosol optical depth (AOD) based on the Moderate Resolution Imaging Spectroradiometer corroborates the persistent haze over northern China. Significantly high levels of AOD (>0.8)

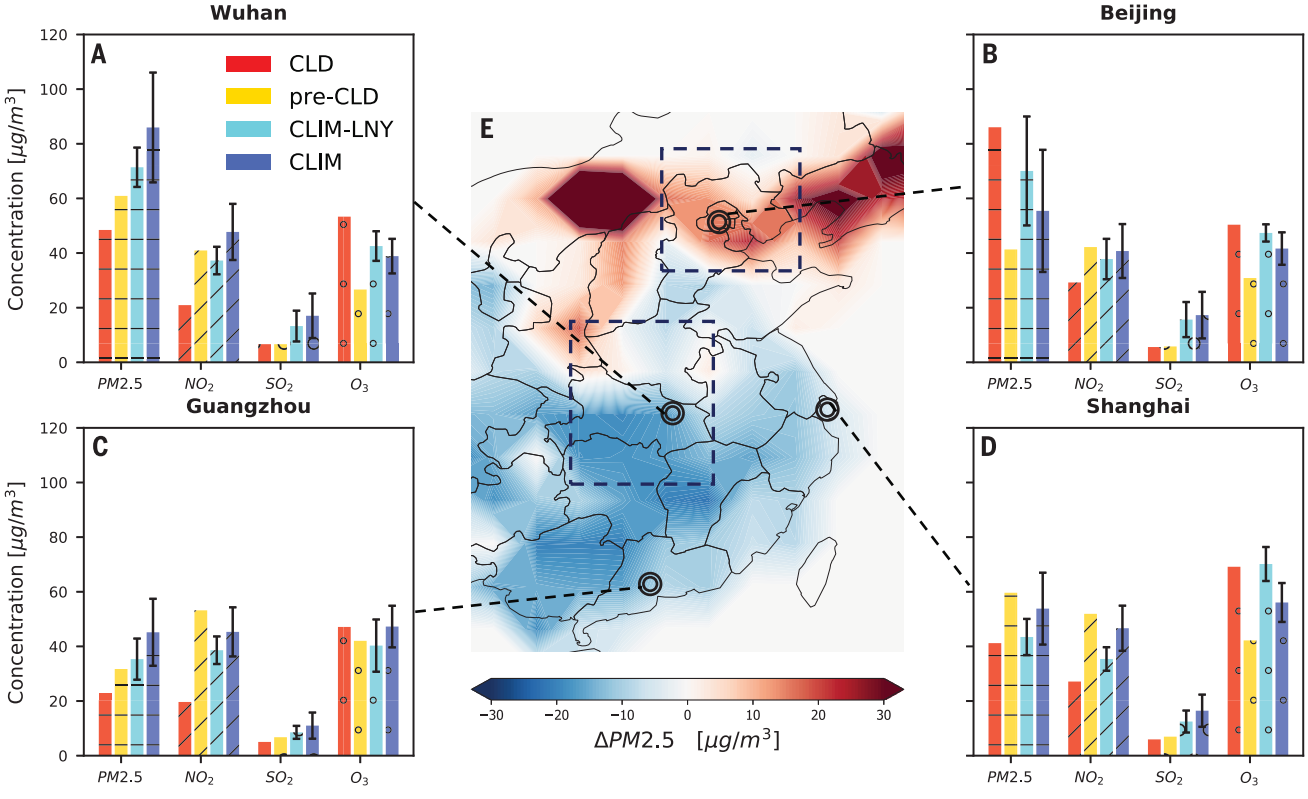

Fig. 2. Ground-based station observation of $PM_{2.5}$, NO_2, SO_2, and ozone in eastern China, including four megacities. (**A**) Wuhan. (**B**) Beijing. (**C**) Guangzhou. (**D**) Shanghai. The figure compares the 3-week averages during the city lockdown period (CLD), the 3-week averages before 2020-CLD (pre-CLD), the 5-year climatology for 2015 to 2019 during the same period of 2020-CLD in the Chinese lunar calendar that covers the Lunar New Year (CLIM-LNY), and the 5-year climatology for 2015 to 2019 during the same period with 2020-CLD in the Gregorian calendar (CLIM). Error bars indicate SDs over multiple years. (**E**) Map of surface $PM_{2.5}$ changes in 2020-CLD compared with CLIM-LNY based on the 1515 state monitoring stations (fig. S2). The low-resolution patterns in the north and west are caused by the sparsity of stations. Two boxes indicate the BTH and central China regions. For ozone, 1 μg m^{-3} is ~0.47 ppb under a standard condition.

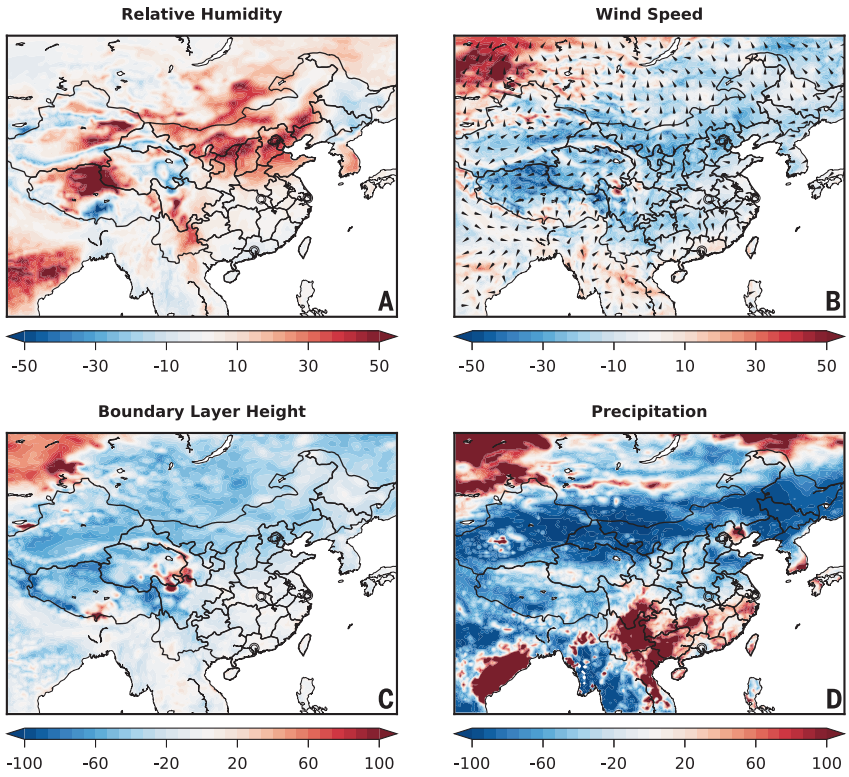

Fig. 3. Fractional changes (%) in meteorological conditions between the 2020-CLD and CLIM-LNY during 2015 to 2019 based on the ERA5 reanalysis data. (**A**) Relative humidity of 1000 hPa, (**B**) 10-m wind speed (contours) and wind direction (vectors), (**C**) boundary-layer height, and (**D**) daily precipitation. Symbols in the maps indicate the location of the four major cities in Fig. 2.

were present over the North China plain but did not occur in any previous year since 2015 (fig. S4), leading to 40 to 100% increases in AOD during the city lockdown.

Possible factors that explain enhanced $PM_{2.5}$ and ozone levels in the face of declining precursor gas emissions include the complex chemistry of secondary aerosols and ozone (*7*, *13*) as well as the meteorological influence (*8*). Changes in relative humidity (RH), near-surface wind speed and direction, planetary boundary layer (PBL) height, and precipitation between the 2020-CLD and CLIM-LNY are shown in Fig. 3, based on fifth-generation European Centre for Medium-Range Weather Forecasts (ECMWF) global atmospheric reanalysis (ERA5). In northern China, which is climatologically dry during the winter, a larger than usual amount of moisture accumulated near the surface during the city lockdown, with a 3-week mean RH of 55.2% and a maximum of 100%. Compared with the climatology, RH increased by 30 to 50% (Fig. 3A), facilitating multiphase reactions for aerosol formation and growth (*16*). Wind conditions were also favorable for haze formation; in Beijing, the mean wind speed decreased by 20%, and winds that normally originate from the polluted industrial regions in Hebei Province switched to southerly (Fig. 3B). Consistent with the increase in RH and the decrease in wind speed, PBL height in northern China generally declined during the city lockdown, inducing a stable boundary layer and stagnant air (Fig. 3C). As a result, both ozone and $PM_{2.5}$ increased in Beijing. During the same period, as precipitation occurred mainly over southern China, no anomalous washout occurred in northern China, conducive for haze development during the city lockdown. Also, as positive feedback to the meteorological variations (*17*), aerosols can reduce PBL height and stabilize the lower atmosphere through their radiative effects (*18*) and suppress light precipitation through their microphysical effects (*19*).

To reveal the physical and chemical mechanisms of the unexpected $PM_{2.5}$ and ozone enhancement in northern China during the COVID-19 outbreak, we have conducted atmospheric chemistry and transport simulations using the Weather Research and Forecast model online coupled with full gaseous and aerosol chemistry (WRF-Chem). The unusual particulate levels during the 2020-CLD in the Beijing-Tianjin-Hebei area (BTH) are well reproduced in our baseline simulations, in terms of consistent peak values of ~200 $\mu g\ m^{-3}$, well-simulated temporal evolution over the 3 weeks, and small mean bias (MB) of ~2.6 $\mu g\ m^{-3}$ (Fig. 4A). Surface ozone concentrations and diurnal cycles are comparable with ground-based observations (Fig. 4B), as with other precursor trace gases, including SO_2, NO_2, and CO (fig. S5). Predicted aerosol chemical composition shows that organic aerosol (OA), nitrate, and sulfate are predominant species in BTH (fig. S6). When severe haze forms with a stable boundary layer and high humidity, inorganic fractions markedly increase with reduced OA, consistent with previous observations in the same area (*20*).

A series of model sensitivity simulations was conducted using altered emission rates, different meteorological conditions, and different sophistication of chemical schemes. An 80% NO_x emission reduction from all sectors in the model, consistent with the observed NO_2 reduction during the city-lockdown period, induces a 13.0% reduction in nitrate aerosol but 26.3% and 15.1% increases in sulfate and secondary OA (SOA), respectively (Fig. 4C). The latter increases can be attributed to the enhanced atmospheric oxidizing capacity after the 42.9% ozone increase (Fig. 4D). The net $PM_{2.5}$ change by NO_x reduction is not evident because of the cancellation of changes in different aerosol components. The meteorological influence on $PM_{2.5}$ and ozone is assessed by comparing a pair of simulations with the meteorological conditions from this year and a multiyear climatology during the same period. It shows that, because of the adverse ventilation conditions and anomalously high humidity during the city-lockdown period, all aerosol species are increased, with the largest fractional change of 63.5% for sulfate (Fig. 4C). Total $PM_{2.5}$ is increased by 31.3% accordingly. Moreover, heterogeneous chemistry processes (materials and methods) contribute positively to the aerosol formation and haze development during the city-lockdown period, because of the concurrent high humidity and aerosol water. Our model assessment shows a 12.0% increase in $PM_{2.5}$ contributed from heterogeneous chemistry in northern China. Comparisons among the simulations altering emissions, chemistry, and meteorology reveal that the previously unseen NO_x reduction during the COVID-19 outbreak does not significantly reduce aerosol formation, because of the nonlinear ozone and aerosol chemistry. In addition, meteorological variations are crucial in the haze formation in northern China by trapping pollutants in the urban area and inducing more efficient aerosol formation from heterogeneous chemistry. Because high humidity and atmospheric stability were absent over central China, including Wuhan, a gradual decline of $PM_{2.5}$ during the lockdown period can be seen in both ground-based observations and model simulations (fig. S7). An increasing trend of ozone can also be identified in the temporal evolution. Aerosol chemical compositions generally are

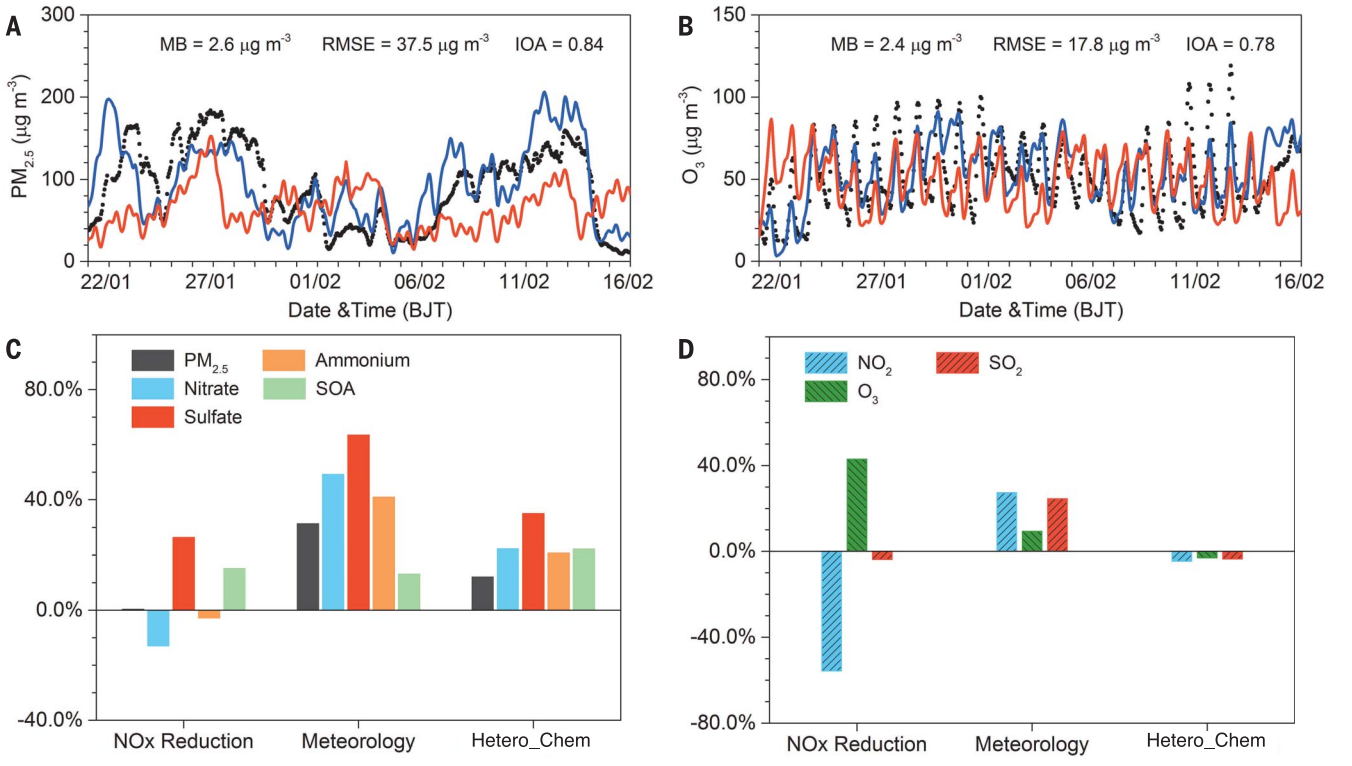

Fig. 4. WRF-Chem simulated aerosol species and precursor gases during the COVID-19 city lockdown period in the BTH region and their sensitivity to the altered emissions, meteorological conditions, and chemical pathways. (**A**) Time evolution of surface $PM_{2.5}$ concentrations in the ground-based observations (black dots), the baseline simulation (blue line), and the sensitivity simulation with the climatological (2015 to 2019) meteorological conditions (red line) (table S3). BJT, Beijing time; IOA, index of agreement; RMSE, root mean square error. (**B**) Same with (A) but for ozone. (**C**) Simulated fractional changes in different aerosol species in response to changes in NO_x emissions, meteorological conditions, and the representation of heterogeneous chemistry. (**D**) Same with (C) but for gaseous pollutants including NO_2, SO_2, and O_3.

maintained, with OA accounting for 36 to 40% of total aerosol mass and sulfate-nitrate-ammonium for another 40% (fig. S6).

The COVID-19 outbreak led to previously unseen anthropogenic emission reductions from traffic and manufacturing sectors and the consequent city lockdowns. Hence, it offered an opportunity to assess the interplay between emissions, chemistry, and meteorology. Our synergistic analyses of the spatiotemporal distributions of PM and precursor gases, meteorological fields, and simulated PM formation pathways reveal a surprising PM exacerbation due to the unfavorable meteorological conditions, invigorated heterogeneous chemistry, and enhanced secondary aerosol formation with the elevated ozone oxidation capacity by NO_x reduction. In particular, our work provides unambiguous evidence that reduction in aerosol precursor emissions was compromised by multiphase chemistry promoted by increased humidity. The role of multiphase chemistry in haze formation is presently uncertain, and the findings in this study call for future research in this area.

Reductions in NO_x and SO_2 from traffic and manufacturing sectors have long been considered as the normal protocol in implementing regulatory policies. Our work shows that such a protocol achieves only limited effects on PM and ozone levels, without simultaneous emission controls from power plants and heavy industry, such as petrochemical facilities. Therefore, we suggest a more comprehensive regulation of precursor gases from all possible sectors when developing an emission control strategy. For example, our model sensitivity experiments show a 20% reduction in ozone and 5% reduction in $PM_{2.5}$ by implementing 30% reductions of VOCs from all possible emission sources (fig. S8). As opposed to the previous Olympic Blue and APEC Blue shutdowns, an unexpected increase in PM levels in northern China occurred in a 3-week period during the COVID-19 pandemic. The decisive role of meteorology in this unexpected haze formation in northern China during this episode underscores the importance of taking meteorological factors into account when short-term stringent emission controls are planned.

As the COVID-19 pandemic is still ongoing, the unexpected PM elevation has potentially profound implications for the airborne transmission of virus (*21*). An emerging study shows plausible virus transmission through aerosols in populous areas (*22*). Meanwhile, exposure to high levels of PM can cause adverse effects on the respiratory and cardiovascular systems and possibly increase the fatality rate of COVID-19. Therefore, future work is urgently needed to establish the causal relationship between aerosol pollution and COVID-19.

REFERENCES AND NOTES

1. Z. An *et al.*, *Proc. Natl. Acad. Sci. U.S.A.* **116**, 8657–8666 (2019).
2. B. Zhao *et al.*, *Proc. Natl. Acad. Sci. U.S.A.* **115**, 12401–12406 (2018).
3. Q. Zhang *et al.*, *Proc. Natl. Acad. Sci. U.S.A.* **116**, 24463–24469 (2019).
4. G. Li *et al.*, *Atmos. Chem. Phys.* **17**, 2759–2774 (2017).
5. K. Li *et al.*, *Proc. Natl. Acad. Sci. U.S.A.* **116**, 422–427 (2019).
6. G. Wang *et al.*, *Proc. Natl. Acad. Sci. U.S.A.* **113**, 13630–13635 (2016).
7. F. Zhang *et al.*, *Proc. Natl. Acad. Sci. U.S.A.* **117**, 3960–3966 (2020).
8. L. Mao *et al.*, *Natl. Sci. Rev.* **6**, 515–523 (2019).
9. S. Wang *et al.*, *Environ. Sci. Technol.* **44**, 2490–2496 (2010).
10. K. Huang, X. Zhang, Y. Lin, *Atmos. Res.* **164–165**, 65–75 (2015).
11. R. Meng *et al.*, *Remote Sens.* **7**, 15224–15243 (2015).
12. D.-Y. Gong *et al.*, *J. Geophys. Res. Atmos.* **119**, 6306–6324 (2014).
13. J. H. Seinfeld, S. N. Pandis, *Atmospheric Chemistry and Physics: From Air Pollution to Climate Change* (Wiley, 2016).
14. M. Levy *et al.*, *Atmos. Environ.* **94**, 231–240 (2014).
15. J. Wu *et al.*, *Proc. Natl. Acad. Sci. U.S.A.* **117**, 9755–9761 (2020).
16. X. Tie *et al.*, *Sci. Rep.* **7**, 15760 (2017).
17. Z. Li *et al.*, *J. Geophys. Res. Atmos.* **124**, 13026–13054 (2019).
18. Y. Wang, A. Khalizov, M. Levy, R. Zhang, *Atmos. Environ.* **81**, 713–715 (2013).

19. Y. Wang, P.-L. Ma, J. H. Jiang, H. Su, P. J. Rasch, *J. Geophys. Res. Atmos.* **121**, 5878–5887 (2016).
20. S. Guo *et al*., *Proc. Natl. Acad. Sci. U.S.A.* **117**, 3427–3432 (2020).
21. R. Zhang, Y. Li, A. L. Zhang, Y. Wang, M. J. Molina, *Proc. Natl. Acad. Sci. U.S.A.* **117**, 14857–14863 (2020).
22. Y. Liu *et al*., *Nature* **582**, 557–560 (2020).

ACKNOWLEDGMENTS

We are grateful to C. Liu and A. Lyapustin for helpful discussions on the satellite products and Y. Wang and Y. Huang for chemistry analysis. **Funding:** Y.W. and Y.L.Y. acknowledge the support of the Jet Propulsion Laboratory, California Institute of Technology, under contract with NASA. Additional support was provided by the NSF (grant AGS-1700727). G.L. and L.L. acknowledge the National Key R&D Plan (grant 2017YFC0210000) and the Strategic Priority Research Program of the Chinese Academy of Sciences (grant XDB40030203). **Author contributions:** Y.W. conceived and designed the research. T.L., Y.W., and Y.L.Y. performed the data analyses and produced the figures. L.L., Y.W., and G.L. performed and analyzed the WRF-Chem simulations. J.Y. and L.L. obtained the ground-based pollution data. Y.W. and J.H.S. wrote the paper. All authors contributed to the scientific discussions and preparation of the manuscript. **Competing interests:** The authors declare no competing interests. **Data and materials availability:** All data are available in the manuscript or the supplementary materials.

SUPPLEMENTARY MATERIALS

science.sciencemag.org/content/369/6504/702/suppl/DC1
Materials and Methods
Figs. S1 to S9
Tables S1 to S3
References (*23*–*41*)

16 March 2020; accepted 9 June 2020
Published online 17 June 2020
10.1126/science.abb7431

Science

Unexpected air pollution with marked emission reductions during the COVID-19 outbreak in China

Tianhao Le, Yuan Wang, Lang Liu, Jiani Yang, Yuk L. Yung, Guohui Li and John H. Seinfeld

Science **369** (6504), 702-706.
DOI: 10.1126/science.abb7431originally published online June 17, 2020

Air pollution epidemic

The lockdown enforced in most cities in China in response to the outbreak of severe acute respiratory syndrome coronavirus 2 (SARS-CoV-2) resulted in the virtual absence of motor vehicle traffic and sharply reduced manufacturing activity for several weeks. Le *et al.* report some of the anticipated and unanticipated effects that this had on air pollution there, including unexpectedly high levels of particulate matter abundances and severe haze formation in some areas. This natural experiment will help in the assessment of air pollution mitigation strategies.

Science, this issue p. 702